

Microwave detected, microwave-optical double resonance of NH_3 , NH_2D , NHD_2 , and ND_3 . II. Predissociation dynamics of the \tilde{A} state

Steven A. Henck,^{a)} Martin A. Mason, Wen-Bin Yan,^{b)} and Kevin K. Lehmann
Department of Chemistry, Princeton University, Princeton, New Jersey 08544

Stephen L. Coy
Harrison Regional Spectroscopy Laboratory, Massachusetts Institute of Technology, Cambridge, Massachusetts 02139

(Received 4 October 1994; accepted 8 December 1994)

Using microwave detected, microwave-optical double resonance, we have measured the homogeneous linewidths of individual rovibrational transitions in the \tilde{A} state of NH_3 , NH_2D , NHD_2 , and ND_3 . We have used this excited state spectroscopic data to characterize the height of the dissociation barrier and the mechanisms by which the molecule uses its excess vibrational and rotational energies to help overcome this barrier. To interpret the observed vibronic widths, a one dimensional, local mode potential has been developed along a N–H(D) bond. These calculations suggest the barrier height is roughly 2100 cm^{-1} , approximately 1000 cm^{-1} below the *ab initio* prediction. The observed vibronic dependence of levels containing two or more quanta in ν_2 is explained by a Fermi resonance between $2\nu_2$ and the N–H(D) stretch. This interaction also explains the observed trends due to isotopic substitution. The rotational enhancement of the predissociation rates in the NH_3 2^1 level is dominated by Coriolis coupling while for the same level in ND_3 , centrifugal effects dominate. © 1995 American Institute of Physics.

I. INTRODUCTION

Although the electronic excited states of most molecules are known to predissociate, the exact mechanisms of these processes remain largely undetermined. The difficulty in modeling molecular predissociation is that the predissociation is usually caused by a coupling of a bound excited electronic state to another electronic state in which the nuclear motion is not bound.² The rate of dissociation depends upon the properties of both electronic states, as well as the nonadiabatic coupling between them. In contrast, the rate of predissociation of the ammonia \tilde{A} state is determined by the rate of crossing over, or tunneling through, a small barrier on a single potential energy surface.³ While a conical intersection exists well beyond this barrier, this intersection effects only the product state distribution and not the predissociation rate. Since knowledge of only a single electronic surface is needed to understand the \tilde{A} state predissociation, it represents one of the most theoretically tractable chemical reactions.

The nature of the barrier to \tilde{A} state dissociation is well understood. In an early *ab initio* self-consistent field and configuration interaction study, the \tilde{A} state was shown to result from excitation to the $4a'_1$ molecular orbital (MO) which continuously changed from a predominantly $3s$ Rydberg orbital at the equilibrium conformation to a hydrogen $1s$ atomic orbital at large H_2N –H separation.³ A small barrier exists along this coordinate due to the change from Rydberg to antivalence character of this orbital as an N–H bond was stretched. The magnitude of this barrier was also shown to be a minimum for planar geometry and to increase with out-of-

plane deformation. The minimum barrier height remains a controversial quantity. In the initial *ab initio* study by Runau *et al.*,³ the barrier was predicted to lie 4600 cm^{-1} above the \tilde{A} state minimum while a more involved theoretical calculation that allowed the H–N–H angle to relax has predicted this barrier to lie at 3200 cm^{-1} .⁴ Semiclassical trajectories predict it lower by an additional 1200 cm^{-1} .⁵ An accurate determination of this barrier height is essential to correctly understand the predissociation mechanisms. Hence, its determination was a primary goal of the present work.

Besides the exhaustive theoretical effort,^{3–10} an extensive experimental effort has also been directed toward characterizing the barrier height and predissociation mechanisms.^{5,11–23} Due to the lack of rotational data as discussed in the previous paper, much of the current understanding of the predissociation mechanism(s) has been extracted by interpreting the vibronic dependence of the predissociation lifetimes. In particular, Vaida and co-workers²⁰ observed a single fourteen member progression in the absorption spectrum of NH_3 and ND_3 in a seeded supersonic jet. Inhomogeneous broadening was sufficiently reduced such that for each vibronic member of this progression, an average rovibrational predissociation rate was extracted. In agreement with the *ab initio* predictions,³ for both isotopomers, the predissociation rates were observed to be slowest for the 2^1 level due to the strong dependence of the barrier height on out-of-plane deformation. Above this level for both species, the predissociation rate was observed to be enhanced greatly by increasing ν_2 excitation. They postulated that for these higher lying levels anharmonic interactions were coupling energy from the bound bending coordinate to the unbound dissociation coordinate, thus, circumventing the barrier. Due to the strong anharmonicity of the \tilde{A} state potential, only a limited amount of information

^{a)}Present address: Texas Instruments, 13536 N. Central Expy., MS 992, Dallas, TX 75243.

^{b)}Present address: Energia, Inc., P. O. Box 1468, Princeton, NJ 08542.

about the barrier is likely to be revealed through the study of these higher lying levels.

Deuterium substitution has been shown to reduce the predissociation rate in \tilde{A} state ammonia substantially and particularly in the lowest few vibronic levels.^{12,16,20} Thus, determining predissociation lifetimes as a function of the number of hydrogens substituted should be a sensitive measure of the barrier height. This effect is attributed to the slower tunneling rates of the deuterium compared to hydrogen as well as slower tunneling rates due to the lower zero-point energy of the N–D stretching modes.²⁴ If one neglects the interaction among the three equivalent N–H(D) bands, the dissociation rate would be the sum of tunneling rates through the three equivalent barriers and each subsequent deuterium substitution would result in an approximate constant decrease in predissociation rate. Such an effect has been observed in the \tilde{A} state action spectra from photodissociation through the 2^1 level.²⁴ At even greater excitation, coupling of vibrational energy into the dissociation coordinate would be expected to enhance the dissociation rate, since it provides a mechanism to “go over the top” of the barrier. Such resonances will depend sensitively on the frequencies of the individual modes involved such that a simple isotopic dependence would not be expected. The effect of any vibration–rotation interactions on the dissociation rate may also lead to a more complex isotopic dependence.

Since the lowest two vibronic levels could only predissociate by tunneling through this barrier, it was anticipated that a better picture of the barrier would be revealed through an understanding of the predissociation in the lowest few vibronic levels. Hence, these levels have been probed by a host of experimental techniques including absorption,¹⁶ two photon fluorescence excitation (2PFE),¹² and rotational resonance Raman excitation profiles (RRREP).²⁵ This work has established a weak predissociation dependence on rotational level. This rotational dependence has been quantitatively fit to a model incorporating a centrifugal modification to the barrier height.^{12,25} However, the much stronger rotational dependence observed in the RRREP’s could have also been described by Coriolis forces.²⁵ These two different mechanisms could not be distinguished since the results of these experiments represent an average increase among all K sub-levels such that distinguishing between the two different mechanisms is difficult.

Fully rotationally resolved spectra have been recorded by optical–optical double resonance methods.^{5,22} However, these experiments were not able to establish a significant predissociation dependence on rotational level. It should be noted that one step of this double resonance scheme involves a multiphoton excitation that might be expected to distort the observed line shapes. Thus, due to the experimental uncertainty of the determined linewidths in these experiments, a weak predissociation dependence on rotational level might have been masked.

Microwave detected, microwave-optical double resonance has recently been used to probe the dynamics in the NH₃ \tilde{A} state 2^0 band.¹⁷ The rotational dependence observed in this level was again quantitatively fit using the centrifugal model.²⁶ In the previous paper, we reported the $\tilde{A} \leftarrow \tilde{X}$ tran-

sition frequencies measured by MODR for the higher lying vibrational levels of the NH₃ \tilde{A} state as well as for the isotopomers.²⁷ This technique has also enabled us to measure the homogeneous linewidths for individually resolved J_K rovibronic transitions for the entire isotopomeric series. Our observed linewidths are considerably narrower than previous reports.^{5,22} Thus, it was hoped that these results would enable us to discern for the various isotopomers the vibrational and rotational contributions to the \tilde{A} state predissociation mechanisms.

Assuming that stretching motions are more correctly described by a local mode coordinate system rather than a normal mode one, a crude one-dimensional potential was designed along an N–H(D) internal bond coordinate. This potential has been used to demonstrate that a 2-1 Fermi resonance between ν_2 and ν_1 quantitatively predicts the observed linewidths for levels with more than one quantum in ν_2 . For the lowest two levels, predissociation could only occur by tunneling through this barrier. To reproduce the observed linewidths of the vibrationless levels in NH₃ and ND₃, the barrier height was reduced roughly 1000 cm⁻¹ relative to the *ab initio* value. This result agrees with the conclusion of Dixon²⁸ who also has demonstrated that the *ab initio* calculations⁴ overestimate the barrier. The predissociation efficiency was also shown to be weakly dependent upon rotation. Surprisingly, this rotational dependence was found to be isotope dependent. For the hydrogen containing isotopomers, the rotational dependence was more adequately described by Coriolis forces coupling energy from ν_2 and into ν_3 and ν_4 , while for ND₃, this rotational dependence obeyed the centrifugal model. This difference arises from the fact that in NH₃ one quantum of ν_2 added to the N–H zero-point energy is isoenergetic with scattering states above the barrier to dissociation while for ND₃ this energy still lies below the top of the barrier. Thus, for ND₃, the Coriolis contribution to the predissociation rate is reduced such that tunneling remains the dominant predissociation pathway.

II. EXPERIMENT

The recording and analysis of the MODR and RFODR data was described in the previous paper and will not be repeated here. The linewidths obtained from such an analysis are given in Tables I–IV. As suggested by Ziegler,²⁵ the observed widths were fit to,

$$\Gamma = \Gamma_0 \times \exp\{\Gamma_B[J(J+1) - K^2] + \Gamma_C K^2\}, \quad (1)$$

where Γ is the observed width, Γ_0 is a determined constant for a given vibronic band, Γ_B reflects the enhancement by rotation in the plane of the molecule, and Γ_C that of the enhancement due to rotation about the symmetry axis. For the asymmetric top species, K^2 is replaced by $\langle J_z^2 \rangle / \hbar^2$, calculated from the fitted rotational constants. In these fits, the observed widths were weighted by the reciprocal of the squared uncertainty predicted by the line shape fit. Results are given in Table V. Because the microwave probe transitions are Q branch lines of the inversion band, our data is primarily for high K lines. For the mixed isotopomer data, we were not able to determine the rotational dependence of the widths due to the limited number of transitions observed

TABLE I. Linewidths of the NH₃ $\tilde{A}\leftarrow\tilde{X}$ state MODR transitions.

Transition	HWHM (cm ⁻¹)	1 σ
	2 ⁰ band	
Q ₂ (2)	16.83	0.06
R ₂ (2)	19.38	0.21
Q ₃ (3)	17.90	0.05
R ₃ (3)	19.37	0.22
Q ₄ (4)	18.81	0.11
Q ₄ (5)	18.11	0.25
R ₄ (5)	24.20	3.60
Q ₅ (5)	19.19	0.13
R ₅ (5)	25.98	0.99
Q ₆ (6)	19.48	0.08
R ₆ (6)	33.31	1.52
P ₆ (7)	16.27	1.57
Q ₆ (7)	20.79	0.14
R ₆ (7)	26.48	1.37
Q ₇ (7)	21.04	0.14
R ₇ (7)	23.70	1.88
Q ₈ (8)	21.00	0.11
R ₈ (8)	26.03	2.35
Q ₉ (9)	22.74	0.44
	2 ¹ band	
Q ₁ (1)	15.03	0.07
R ₁ (1)	14.82	0.15
P ₂ (3)	12.73	0.16
Q ₂ (3)	15.39	0.05
R ₂ (3)	15.99	0.08
Q ₃ (3)	15.07	0.02
R ₃ (3)	15.48	0.09
P ₂ (5)	13.88	0.33
Q ₂ (5)	15.56	0.45
R ₂ (5)	17.24	0.27
P ₄ (5)	13.64	0.14
Q ₄ (5)	19.65	0.16
R ₄ (5)	16.35	0.06
Q ₄ (5)	14.75	0.43
R ₄ (5)	17.68	0.31
P ₃ (6)	18.27	0.35
Q ₃ (6)	12.10	0.81
R ₃ (6)	16.75	0.08
P ₅ (6)	18.98	0.54
Q ₅ (6)	11.09	0.54
R ₅ (6)	17.14	0.08
R ₆ (7)	21.28	0.54
Q ₇ (8)	17.93	0.15
Q ₈ (8)	16.04	0.03
R ₈ (8)	20.10	0.79
P ₈ (9)	46.17	6.61
R ₈ (9)	23.22	2.33
Q ₉ (9)	14.64	0.09
R ₉ (9)	33.74	5.11
	2 ² band	
Q ₃ (3)	22.08	0.27
R ₃ (3)	26.02	1.36
Q ₆ (6)	20.09	0.16
R ₆ (6)	21.92	4.07
	2 ³ band	
Q ₁ (1)	42.37	0.58
Q ₂ (2)	45.30	0.64
Q ₃ (3)	45.33	0.30
Q ₃ (4)	47.32	0.72
Q ₄ (4)	53.33	0.35
Q ₃ (5)	48.36	0.23
Q ₅ (5)	49.66	0.53
Q ₃ (6)	47.94	0.71

TABLE I. (Continued.)

Transition	HWHM (cm ⁻¹)	1 σ
Q ₆ (6)	46.91	0.33
Q ₆ (7)	48.53	0.22
Q ₇ (7)	44.54	0.24
Q ₆ (8)	45.41	0.61

in these molecules. For the asymmetric tops, the ground state Q branch is widely spread, reducing the number of strong transitions in the region covered by our microwave equipment.

III. DISCUSSION

A. Empirical local mode potential surface

The \tilde{A} state absorption spectrum has been modeled as a two symmetric mode problem.^{7,8} One quantum of stretching excitation contains more energy than needed to overcome the barrier along a single N-H bond, yet the ν_1 normal mode coordinate is still strongly bound. The dissociation reaction coordinate is a mixture of ν_1 and the two components of the

TABLE II. Linewidths of the NH₂D $\tilde{A}\leftarrow\tilde{X}$ state MODR transitions.

Transition	HWHM (cm ⁻¹)	1 σ
	2 ⁰ band	
3 ₀₃ \leftarrow 3 ₁₃	17.46	0.10
4 ₂₃ \leftarrow 3 ₁₃	17.46	0.10
4 ₁₄ \leftarrow 4 ₀₄	17.41	0.10
5 ₁₄ \leftarrow 4 ₀₄	17.41	0.10
5 ₁₅ \leftarrow 5 ₀₅	18.57	0.18
6 ₁₅ \leftarrow 5 ₀₅	18.57	0.18
6 ₀₆ \leftarrow 7 ₁₆	22.85	0.46
7 ₂₆ \leftarrow 7 ₁₆	22.85	0.46
7 ₀₇ \leftarrow 8 ₁₇	18.97	0.18
8 ₂₇ \leftarrow 8 ₁₇	18.97	0.18
9 ₂₇ \leftarrow 8 ₁₇	19.47	1.32
	2 ¹ band	
3 ₁₃ \leftarrow 3 ₀₃	11.74	0.04
4 ₁₃ \leftarrow 3 ₀₃	12.27	0.26
4 ₀₄ \leftarrow 4 ₁₄	12.21	0.14
5 ₂₄ \leftarrow 4 ₁₄	12.21	0.14
5 ₀₅ \leftarrow 5 ₁₅	12.43	0.09
6 ₂₅ \leftarrow 5 ₁₅	20.33	1.53
6 ₁₆ \leftarrow 7 ₂₆	10.35	1.11
7 ₁₆ \leftarrow 7 ₂₆	13.54	0.14
8 ₃₆ \leftarrow 7 ₂₆	11.83	0.73
7 ₁₇ \leftarrow 8 ₂₇	11.64	0.94
8 ₁₇ \leftarrow 8 ₂₇	13.74	0.08
9 ₃₇ \leftarrow 8 ₂₇	15.27	0.74
	2 ² band	
3 ₀₃ \leftarrow 3 ₁₃	21.30	0.12
4 ₂₃ \leftarrow 3 ₁₃	21.30	0.12
4 ₁₄ \leftarrow 4 ₀₄	19.60	0.28
5 ₁₅ \leftarrow 5 ₀₅	21.85	0.13
6 ₁₅ \leftarrow 5 ₀₅	21.85	0.13
7 ₂₆ \leftarrow 7 ₁₆	20.48	0.78
7 ₀₇ \leftarrow 8 ₁₇	7.83	3.43
8 ₂₇ \leftarrow 8 ₁₇	21.62	0.40
9 ₂₇ \leftarrow 8 ₁₇	42.11	7.39

TABLE III. Linewidths of the NHD₂ $\tilde{A} \leftarrow \tilde{X}$ state MODR transitions.

Transition	HWHM (cm ⁻¹)	1 σ
2 ⁰ band		
2 ₀₂ ←2 ₁₂	10.24	0.11
3 ₂₂ ←2 ₁₂	11.12	0.35
3 ₁₃ ←3 ₀₃	9.41	0.17
4 ₁₃ ←3 ₀₃	6.58	0.83
4 ₁₄ ←5 ₂₄	8.18	0.99
5 ₁₄ ←5 ₂₄	10.30	0.12
6 ₃₄ ←5 ₂₄	10.09	0.45
2 ¹ band		
2 ₁₂ ←2 ₀₂	6.45	0.04
3 ₁₂ ←2 ₀₂	5.95	0.14
3 ₀₃ ←3 ₁₃	6.29	0.05
4 ₂₃ ←3 ₁₃	6.35	0.28
4 ₀₄ ←5 ₁₄	6.66	0.21
5 ₂₄ ←5 ₁₄	6.54	0.03
6 ₂₄ ←5 ₁₄	7.13	0.10
2 ² band		
2 ₀₂ ←2 ₁₂	17.88	0.18
3 ₂₂ ←2 ₁₂	17.88	0.18
3 ₁₃ ←3 ₀₃	18.98	0.28
4 ₁₃ ←3 ₀₃	18.98	0.28
4 ₁₄ ←5 ₂₄	18.99	0.09
5 ₁₄ ←5 ₂₄	18.99	0.09
6 ₃₄ ←5 ₂₄	18.99	0.09

antisymmetric N–H stretching mode, ν_3 . This potential topology will lead to strong nonlinear interaction between the ν_1 and ν_3 normal modes such that an initial state corresponding to ν_1 excitation will rapidly trifurcate into three equivalent wave packets corresponding to bond-breaking along each of the three equivalent N–H(D) bonds. The depth of the exit channels and the sharpness of the motion along the symmetric stretch should lead to little amplitude being reflected back. Thus, one should expect only weak recurrence.²⁹

In work on stable symmetric hydrides, such as the ground state of ammonia, it has been established that one can treat the X–H stretching motion equivalently with either a local mode or normal mode basis. When the single bond anharmonicity dominates over the bond–bond harmonic coupling, the eigenstates are expected to be close to symmetrized local mode states. Contrarily, when the harmonic coupling dominates over anharmonicity, the eigenstates are closer to normal mode basis functions. For perfect harmonic motion, the local mode and normal mode descriptions of the fundamental levels are identical. For the ammonia \tilde{A} state, however, the potential along a single N–H bond is highly anharmonic. In fact, as will be shown below, the zero-point level is the only resonance below the barrier. As a result, excitation of one bond mode leads to dissociation in a single vibrational period (10 fs). The time required for exchange of vibrational energy between the N–H bonds is longer by approximately $f_{rr}/f_{rr'}$, which based upon the *ab initio* harmonic force field⁷ is predicted to be greater than 50. Thus, the \tilde{A} state of ammonia is the “ultimate” local mode molecule, with bond–bond coupling negligible compared to the rate of dissociation if the N–H stretching modes are excited.

TABLE IV. Linewidths of the ND₃ $\tilde{A} \leftarrow \tilde{X}$ state MODR transitions.

Transition	HWHM (cm ⁻¹)	1 σ
2 ⁰ band		
Q ₃ (3)	2.241	0.099
Q ₄ (4)	1.927	0.051
Q ₃ (5)	1.916	0.096
Q ₅ (5)	2.024	0.036
Q ₆ (6)	1.946	0.075
Q ₆ (7)	1.364	0.114
Q ₇ (7)	2.085	0.038
Q ₆ (8)	1.790	0.056
Q ₇ (8)	2.193	0.053
Q ₈ (8)	2.075	0.026
Q ₆ (9)	1.581	0.355
Q ₉ (9)	1.524	0.062
Q ₉ (10)	1.887	0.070
2 ¹ band		
Q ₁ (1)	0.782	0.044
Q ₂ (2)	0.781	0.030
Q ₃ (3)	0.664	0.016
R ₃ (3)	0.742	0.029
Q ₃ (4)	0.749	0.025
Q ₄ (4)	0.765	0.008
R ₄ (4)	0.743	0.059
Q ₃ (5)	0.832	0.053
Q ₅ (5)	0.936	0.033
Q ₃ (6)	1.080	0.053
Q ₅ (6)	1.050	0.036
Q ₆ (6)	1.518	0.019
Q ₆ (7)	0.958	0.017
Q ₇ (7)	1.049	0.014
Q ₆ (8)	1.344	0.021
Q ₇ (8)	1.106	0.050
Q ₈ (8)	1.039	0.012
Q ₃ (9)	1.540	0.137
Q ₆ (9)	1.923	0.127
Q ₉ (9)	1.281	0.031
Q ₉ (10)	1.611	0.029
Q ₉ (11)	1.849	0.058
Q ₁₀ (11)	1.593	0.075
Q ₁₁ (12)	1.598	0.058
Q ₁₂ (14)	1.534	0.086
2 ² band		
Q ₃ (3)	7.226	0.010
Q ₃ (4)	11.592	0.328
Q ₄ (4)	7.660	0.198
Q ₃ (5)	9.423	0.463
Q ₅ (5)	9.941	0.172
Q ₆ (6)	7.640	0.148
Q ₆ (7)	6.814	0.505
Q ₇ (8)	8.789	0.221
Q ₉ (9)	8.352	0.704

As a result, we have modeled the dissociation in terms of three uncoupled, single bond modes.

Figure 1 shows a model potential we have used to fit the observed dissociation rate. The curve contains information from the *ab initio* calculations⁴ as well as from the experimentally measured information about the position of the barrier.²⁷ These values are repeated below.

TABLE V. Constants obtained from a fit of the observed rovibronic linewidths to Equation (1).

	ν_2	Γ_0	Γ_B	Γ_C
NH ₃	0	17.0(4)	0.006(4)	0.0028(9)
	1	14.6(3)	0.007(2)	0.0004(5)
	2	22(1)	0.02(1)	-0.005(2)
	3	47(4)	0.001(4)	-0.001(2)
NH ₂ D	0	17.0(9)		
	1	11.5(3)		
	2	21(1)		
NHD ₂	0	10(1)		
	1	6.4(3)		
	2	17.7(5)		
ND ₃	0	2.1(1)	-0.0048(29)	-0.0016(11)
	1	0.74(5)	0.0058(31)	0.0038(15)
	2	7.7(8)	0.065(11)	-0.0021(47)

$$\begin{aligned}
 r_e & 1.06 \text{ \AA} \\
 r_b & 1.32 \text{ \AA} \\
 \Delta H & 3200 \text{ cm}^{-1} \\
 f_{rr}(r < r_b) & 2.56 \times 10^5 \text{ cm}^{-1}/\text{\AA}^2 \\
 f_{rr}(r_b < r < R) & -3.36 \times 10^4 \text{ cm}^{-1}/\text{\AA}^2.
 \end{aligned}$$

The curve consists of a pair of parabolas whose extrema and curvature are based upon the *ab initio* potential,⁴ but whose barrier height can be adjusted. Beyond some large separation, $R \gg r_e$, the potential was taken to be $-10\,000 \text{ cm}^{-1}$ correlating with the energy difference of the NH₃ \tilde{A} state and the ground states of the photofragments, NH₂ and H.³ The

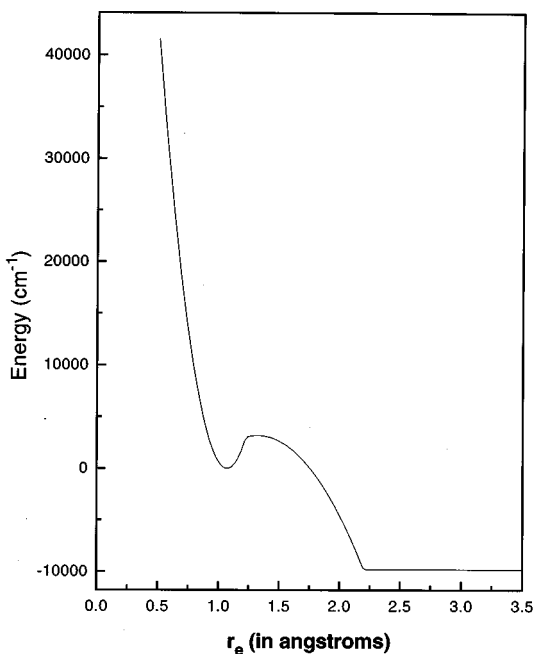


FIG. 1. Model one-dimensional energy surface of the \tilde{A} state of ammonia along the dissociative N-H coordinate. Curve is composed of two parabolas with positions and radius of curvature corresponding to the calculated values.

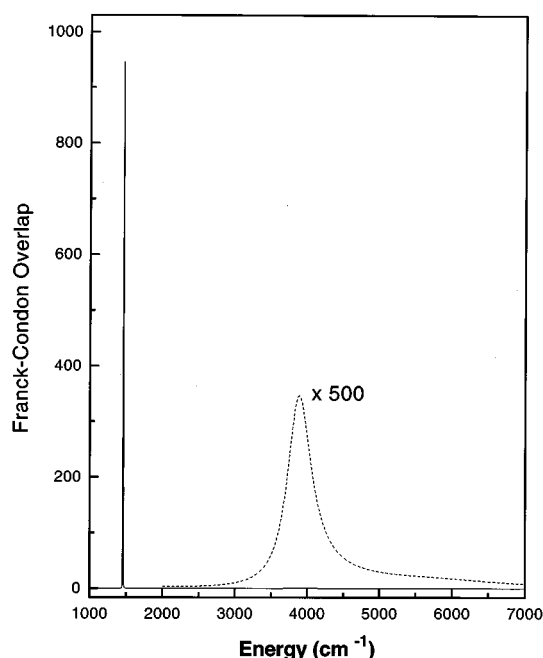


FIG. 2. Predicted Franck-Condon overlap for N-H from ground state wave function. Upper state potential has a 3200 cm^{-1} high barrier to dissociation. First excited state lies above the barrier and lies 2480 cm^{-1} above the zero-point level and has $< 1\%$ of the peak height.

real eigenstates, $\psi(E)$ were calculated at each energy by numerical integration and normalized such that $\int \psi(E) \psi(E') dx = 2\pi \delta(E - E')$.

We begin our discussion with the barrier height picked to agree with the most recent *ab initio* prediction of 3200 cm^{-1} .⁴ In order to mimic what we would expect for ν_1 absorption activity, we calculated the Franck-Condon overlap of $\psi(E)$ with a Gaussian picked to model the zero-point level of the ground electronic state. The resulting squared overlap versus energy is presented in Figure 2. We observe a sharp resonance at 1450 cm^{-1} with a HWHM of 0.16 cm^{-1} . This resonance corresponds to the zero-point level below the dissociation barrier. If this represented the vibrationless level of the \tilde{A} state, one predicts a homogeneous width of three times this size since there are three equivalent hydrogen atoms that could tunnel out; thus, the lifetime broadening will be three times the lifetime broadening of each N-H bond. This prediction is much smaller than the 17 cm^{-1} HWHM measured for the NH₃ origin.

While the features of our crude potential have a clear physical interpretation, this potential overestimates the thickness of the barrier relative to the *ab initio* potential.⁴ As a consistency check, using a spline interpolation, we numerically solved the one-dimensional Schrodinger equation for this potential. Franck-Condon overlap with the ground state wave function resulted in a sharp resonance at 1460 cm^{-1} with a width of 0.73 cm^{-1} in qualitative agreement with the results from our more crude approach. Thus, we justify our simple method and conclude that the *ab initio* calculation has overestimated the barrier height. Dixon reached the same conclusion based upon his two-dimensional wave packet calculations.⁶

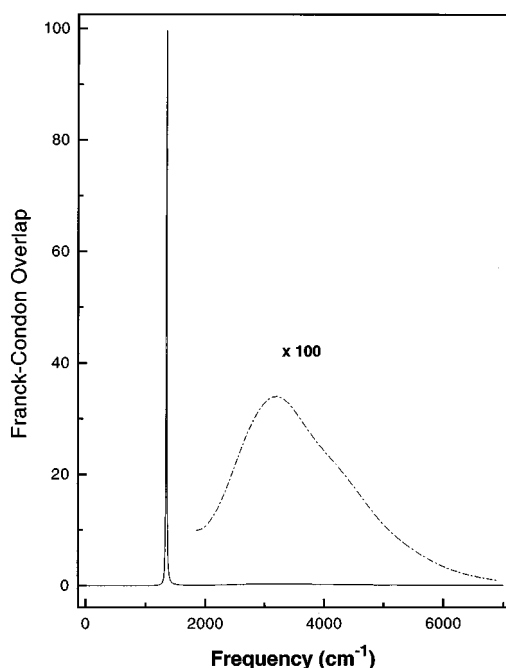


FIG. 3. Predicted Franck-Condon overlap for N-H from ground state wavefunction as a function of energy above T_e . Upper state potential has a 2075 cm^{-1} high barrier to dissociation. The first excited state lies approximately 2000 cm^{-1} above the zero-point level and is approximately 950 cm^{-1} wide.

In order to reproduce the observed 17.1 cm^{-1} width of the NH₃ zero-point transition, the barrier height in our model potential was reduced to 2075 cm^{-1} . Plotted in Figure 3 is the Franck-Condon overlap as a function of energy above T_e for this corrected potential. The zero-point level lies 1350 cm^{-1} above T_e and has a HWHM of 5.7 cm^{-1} per hydrogen in good agreement with the experimental measurement. Thus, in order to model the experimentally measured width of the NH₃ zero-point level, we need to lower the *ab initio* barrier height⁴ by more than 1000 cm^{-1} .

As shown in Figure 3, an extremely broad quaresonance above the barrier is also present. This quaresonance represents what may be called one quantum in the N-H local mode. Eigenstates in this energy region have their inner turning points at bond lengths slightly less than r_e , and thus have significant overlap with the ground state Gaussian. Our crude calculation predicts this resonance lies 3370 cm^{-1} above T_e (2020 cm^{-1} above the zero-point level) and has a 2850 cm^{-1} linewidth. Because of its broad width, the peak absorption is expected to be small relative to the zero-point level, making this level very difficult to detect. Ashfold *et al.*⁵ have measured a 500 cm^{-1} wide resonance centered at 2300 cm^{-1} above the zero-point level that they have assigned to 1¹. As discussed in our previous paper, we have reassigned this band to 4². This level is very likely to be strongly coupled to the N-H stretching modes through Fermi coupling leading to the observed rapid dissociation rate.

Using the same potential, we also calculated the Franck-Condon overlap for an N-D bond. Results from the calculation are presented in Figure 4. The zero-point level is found at 1035 cm^{-1} with a width of 0.16 cm^{-1} per deuterium. The

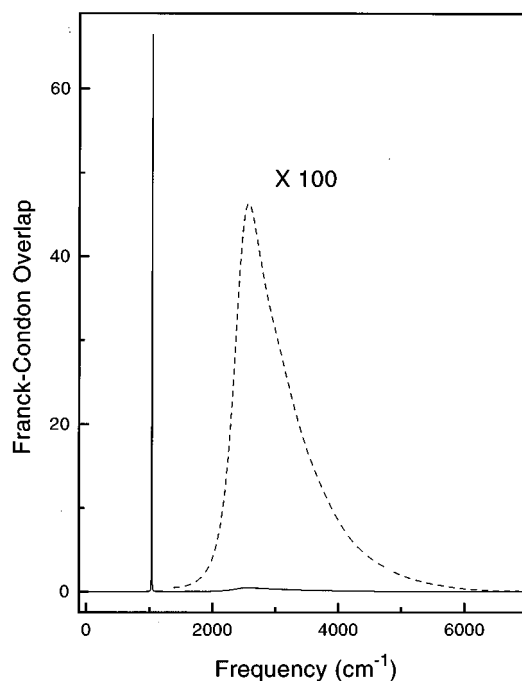


FIG. 4. Predicted Franck-Condon overlap for N-D from ground state wavefunction as a function of energy above T_e . Upper state potential has a 2075 cm^{-1} high barrier to dissociation. The first excited state lies approximately 1700 cm^{-1} above the zero-point level and is approximately 450 cm^{-1} wide.

ND₃ zero-point level is predicted to have a homogeneous linewidth of 0.48 cm^{-1} comparing favorably with the experimental measurement of 0.4 cm^{-1} . We calculate the N-D second resonance to have a homogeneous linewidth of 1360 cm^{-1} and to lie about 2750 cm^{-1} above T_e or about 1720 cm^{-1} above the zero point level. A broad feature was observed at 1790 cm^{-1} in the ND₃ dispersed fluorescence spectrum that has been assigned to the 1¹ band. As for NH₃, we reassign this feature to the 4² band.

A quantitative calculation to test the accuracy of this local mode approximation is clearly desirable. Unfortunately, this calculation would require at a minimum *ab initio* calculations along the three stretching coordinates, and then a three-dimensional wave packet propagation of the ground state Gaussian on this potential. If such a calculation dramatically reduces the predicted resonance widths of the 1¹ level, then we would withdraw our reassignment of the peaks Ashfold *et al.*⁵ assign to 1¹. However, since the basic vibronic and isotopic trends are predicted by this crude potential, we believe our empirical dissociation potential contains the essential features of the true potential.

B. Predissociation dependence upon vibrational level

The increasing dissociation rate with ν_2 excitation above 2¹ suggests that anharmonic interactions are coupling two quanta of vibrational energy out of the bending normal mode into one of the three N-H(D) bond coordinates lying along the dissociation coordinate.²⁰ The lowest order vibrational coupling that could be responsible is a Fermi resonance between ν_2 and ν_1 caused by the k_{hhs} term in a harmonic approximation. We estimate the value of this coupling con-

stant by assuming the molecule vibrates out-of-plane with constant bond length. This approximation is justified by the *ab initio* potential.⁴

Classically, the above coupling leads to a forcing of the stretching mode at two times the frequency of the bending mode. If there is a 2:1 resonance of the harmonic frequencies, one would expect an efficient transfer of energy inside some resonance zone. The experimentally determined force field given in the previous paper does not predict an exact resonance,²⁷ but a small amount of average energy transfer would be expected due to nonresonant coupling. Further, given the rapid dissociation of the N–H(D) stretching modes, their frequencies are poorly defined, making the resonance condition much less restrictive. A 2:1 Fermi resonance implies the transfer of two quanta in ν_2 into one quantum in ν_1 ; anharmonic transfer of one quantum of ν_2 is rigorously symmetry forbidden. We see that this mechanism operates only for levels containing two or more quanta in ν_2 and the rapid increase in linewidth observed above the 2¹ level is predicted.

We use our empirical potential to estimate the expected magnitude of the Fermi resonance. We use as a zero order model, the coupling of two harmonic oscillators and by second order perturbation theory, we find that the average vibrational energy in the stretching coordinate increases by an amount given by,

$$\langle \Delta E_s \rangle = \omega_s \left(\frac{k_{hhs}^2}{4\sqrt{2}} \right) \left[\frac{\nu_2(\nu_2-1)}{(\omega_s-2\omega_2)^2} + \frac{(2\nu_2+1)^2}{\omega_s^2} + \frac{(\nu_2+1)(\nu_2+2)}{(\omega_s+2\omega_2)^2} \right], \quad (2)$$

where ω_s is the stretching frequency, ω_2 is the bending frequency, ν_2 is the number of quanta in the out-of-plane bend, and k_{hhs} is the coupling constant. Using the results from Ziegler,²⁵ the effect of the Fermi resonance on the transition linewidth is

$$\Delta\Gamma = \Gamma_0 \exp\left[\frac{\langle \Delta E_s \rangle}{\hbar\omega_2} \right], \quad (3)$$

where $\hbar\omega_2 = 1063 \text{ cm}^{-1}$ is the imaginary frequency at the top of the barrier. Putting in values estimated from the *ab initio* force field⁷ gives an increase in energy that is far too small to explain the observed vibrational dependence of the widths.

In order to account for the highly anharmonic motion along the N–H(D) stretching coordinates, we use our above estimate for this potential curve. States with two quanta in the out-of-plane bending mode couple directly to scattering states above the dissociation barrier. We use Fermi's Golden rule to estimate the contribution of the coupling to the dissociation rate,

$$k_{\text{diss}} = \frac{4\pi}{\hbar^2} \sqrt{\frac{2m}{E}} \langle V_C \rangle^2, \quad (4)$$

where $\langle V_C \rangle$ is the coupling matrix, E is the energy relative to the bottom of the exit channel, and the $\sqrt{2m/E}$ factor arises due to the density of states and box normalization of the

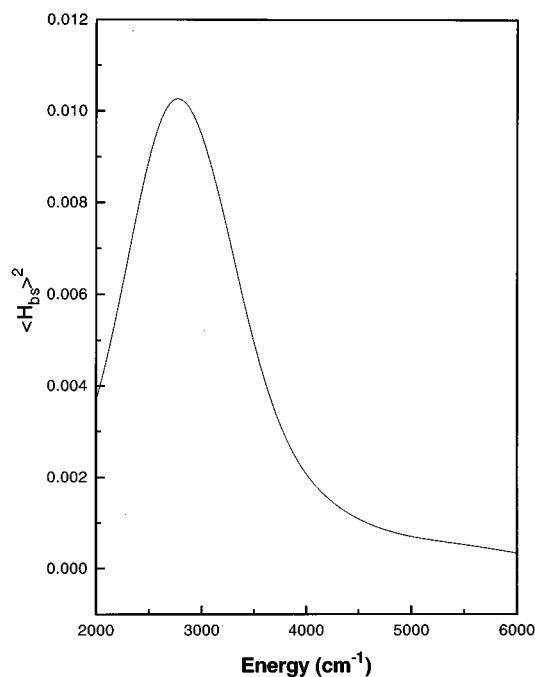


FIG. 5. The squared bend–stretch coupling matrix element for the bend and the stretch versus the energy in a single N–H stretch including the zero-point energy.

wave functions. Assuming the simplest resonance, Fermi coupling between the bend and the stretch is predicted by

$$\langle V_C \rangle = \frac{1}{2} f_{rhh} \langle \nu_2 - 2 | h^2 | \nu_2 \rangle \langle E_0 + \Delta E_2 | (r - r_0) | \Psi_0 \rangle^2, \quad (5)$$

where f_{rhh} is the cubic bend stretch force constant, h is the out-of-plane bend internal coordinate, and $\langle E_0 + \Delta E_2 | (r - r_0) | \Psi_0 \rangle$ is the coupling matrix element. $|\Psi_0\rangle$ is the zero point resonance normalized to unity inside the well and $\langle E_0 + \Delta E_2 |$ is a continuum function normalized to $2\pi \sin(kr)$ in the asymptotic region ($r \gg r_0$). We use the harmonic approximation for the out-of-plane bend and values for f_{hh} from our experimentally estimated force field to determine the expectation value for h^2 . This value was given by

$$\langle \nu_2 - 2 | h^2 | \nu_2 \rangle = 7.614 \times 10^{-3} \sqrt{\nu_2(\nu_2 - 1)} \text{ \AA}^2. \quad (6)$$

Given in Figures 5 and 6 is the squared coupling matrix element as a function of the energy in the N–H(D) bond. Collecting the above expressions along with the *ab initio* value for f_{rhh} of 2.66 aJ/\AA^{37} allowed estimation of the predissociation rates and thus the expected transition linewidths. These calculated values are presented in Table VI along with our measured values.

The predicted dissociation rates are about a factor of three too large for the 2² levels, and increase too rapidly above that. Roughly, the isotopic dependence is correctly predicted. One explanation for the predicted dissociation being much faster than observed is that the *ab initio* value of f_{rhh} may be too large. Even more significant may be our neglect of the barrier dependence on out-of-plane angle. Increasing the barrier height will reduce the coupling matrix

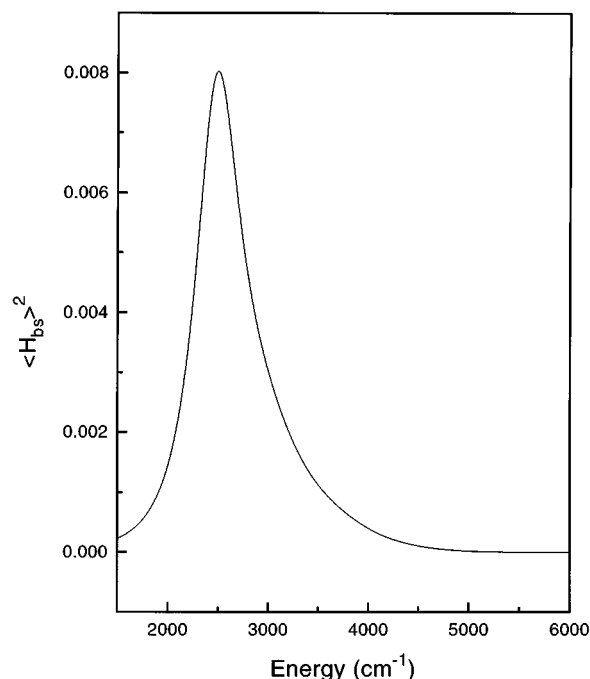


FIG. 6. The squared bend–stretch coupling matrix element for the bend and the stretch versus the energy in a single N–D stretch including the zero-point energy.

element among the zero-point level and the scattering states and decrease the predicted Fermi resonance contribution to the dissociation rate. Consequently, we conclude that our overestimate of the Fermi contribution to the dissociation rate is caused by the neglect of the barrier dependence on out-of-plane deformation. Proper treatment of this problem,

TABLE VI. Linewidths calculated for 2:1 Fermi coupling between the out-of-plane bend and the stretching vibration.

	ν_2	$\Gamma(\text{calc})$	$\Gamma(\text{obs})$
NH ₃	2	66.8	22
	3	160.4	47
	4	244.1	75
NH ₂ D	2	79.0	21
	3	191.5	52
	4	313.3	78
	5	451.5	78
NHD ₂	2	77.7	18
	3	207.5	36
	4	343.2	54
	5	474.6	59
ND ₃	2	37.3	7.6
	3	98.5	
	4	162.5	
	5	267.2	17.5 ^a

^aReference 30.

including both Fermi resonance and the effect of barrier changes with out-of-plane angle, requires two-dimensional wave packet calculations that are beyond our computational resources.

This resonance calculation does rationalize the larger than expected dissociation rate for the NHD₂ isotopomer. Even though there is great uncertainty as to the frequency of the stretching levels, two quanta of ν_2 for NHD₂ would be expected to be in closer resonance with the N–D stretch than for two quanta in any of the other isotopomers, leading to an enhanced dissociation rate. Contrary to the mechanism controlling the dynamics in the tunneling region, this mechanism predicts that the N–D bond dissociates faster than the N–H bonds for these higher lying levels.

C. Predissociation dependence on rotational level

The predissociation dependence on rotational level can arise from two independent sources. In the first mechanism, as extensively discussed by Ashfold *et al.*^{5,12} and Ziegler,²⁵ rotation about either the *b* or *c* axis will promote an N–H(D) bond lengthening resulting in an effective barrier reduction. In the second mechanism, *b* axis rotation causes the ν_2 mode to be coupled to the unbound ν_3 and ν_4 modes through Coriolis forces and, hence, increasing the probability of barrier penetration. If centrifugal effects are the dominant source of rotational enhancement, the ratio of *b* to *c* axis effects should be constant with vibronic excitation. Contrarily, the Coriolis coupling matrix elements would scale with ν_2 . Hence, the two mechanisms can be distinguished by measuring the ratio of *b* to *c* axis effects as a function of ν_2 .

We estimate this ratio allowing only centrifugal effects to contribute. Assuming the dissociating H(D) atom lies on the *y* axis, the effective potential is given by

$$V(\mathbf{r}) = V_0(\mathbf{r}) + \frac{[J(J+1) - K^2]}{4I_x(\mathbf{r})} + \frac{K^2}{2I_z(\mathbf{r})}, \quad (7)$$

where $V_0(\mathbf{r})$ is the rotationless potential and $1/2[J(J+1) - K^2]$ and K^2 are the expectation values for *x* and *z* axis rotation respectively. Using the *ab initio* values for r_e and r_b at 1.055 Å and 1.32 Å, respectively, the rotational correction to the barrier height is estimated to be

$$\Delta V = 1.25[J(J+1) - K^2] + 0.73K^2 \quad (\text{cm}^{-1}). \quad (8)$$

Thus, the centrifugal model predicts a *B* axis effect to *C* axis effect ratio of 1.75. We also note that for the centrifugal model this ratio is independent of the barrier shape and only weakly dependent upon barrier position. For instance, as r_b was varied from r_e to ∞ , this ratio only changed from 2 to 1.

From our NH₃ data, the ratio of *b* axis to *c* axis effects was found to be 2.2 ± 1 . for the zero-point level and $15. \pm 2$. for the 2¹ level. We predict that centrifugal effects dominate in the vibrationless level while Coriolis forces dominate in the 2¹ level. This change in dominant mechanism can be explained utilizing our empirical N–H local mode potential. This potential predicts the zero point energy of an N–H bond mode to be 1350 cm⁻¹ while the barrier height was determined to be 2075 cm⁻¹. The 2¹ level lying roughly 900

cm⁻¹ above this level is expected to lie well above the barrier and therefore be Coriolis coupled to a manifold of continuum states.

Using a procedure similar to the one we used to estimate the magnitude of the Fermi resonance, we estimate the rotational dependence of the linewidths in the NH₃ 2¹ level due to Coriolis forces. In this case, the coupling matrix elements are given by

$$\langle V_C \rangle = -I_{xx}^{-1} \frac{\hbar}{2} \sqrt{J(J+1) - K^2} \zeta_{sb}^x \langle Q_s P_b - Q_b P_s \rangle, \quad (9)$$

where I_{xx} is the moment of inertia about the x axis, ζ_{sb}^x is the stretch-bend Coriolis coupling constant which we set to its ground state value of 0.752, Q_s and Q_b are the normal mode coordinates for the stretch and bend, and P_s and P_b are the conjugate momenta to these normal coordinates. By substituting Equation (9) into Equation (4), we can estimate the Coriolis enhancement to the predissociation rate and the expected linewidth enhancement. The Coriolis contribution to the linewidth was calculated to be

$$\Gamma_0 = 0.11[J(J+1) - K^2]. \quad (10)$$

For the NH₃ 2¹ level, this predicted value is in excellent agreement with the observed *b* axis rotational dependence of 0.10(4) cm⁻¹.

The ND₃ results are more poorly determined than our NH₃ results. We still can compare our determined ratio of *b* axis to *c* axis enhancement for the two isotopomers. In contrast to NH₃, this ratio for the ND₃ 2¹ level was determined to be 2.1(7) more in line with the centrifugal model. Surprisingly, for the two isotopomers, the dominant mechanism for rotational enhancement appears to be different.

To understand this result we again turn to our empirical N-H local mode potential. This potential predicts the zero-point energy in the N-D stretch to be 1035 cm⁻¹. Addition of one quantum in ν_2 with an energy of approximately 670 cm⁻¹ still lies well below the barrier. Since continuum states below the top of the barrier have small amplitude near r_e , the Coriolis coupling matrix element should be much smaller for ND₃ than for NH₃. Therefore, changes in the zero-point energies and mode frequencies due to isotopic substitution are shown to have a dramatic effect on the predissociation dependence on rotational level.

IV. CONCLUSION

We have measured the homogeneous linewidths of individual rovibrational transitions using MODR. Our measured linewidths are considerably narrower than previous determinations.^{5,22} Since the observed widths were much larger than the laser bandwidth or the Doppler width, they represent a direct measure of the predissociation lifetime. Thus, we have used these linewidths to more fully interpret the \tilde{A} state predissociation mechanisms.

Using the available experimental and theoretical data, we have developed a one-dimensional, local mode potential along a N-H(D) bond. This potential has been used to qualitatively predict the vibronic and isotopic dependence of the predissociation rates. In order to simulate the observed

widths in the zero-point levels, the barrier height had to be lowered to 2075 cm⁻¹, about 1000 cm⁻¹ below the *ab initio* prediction.⁴ Dissociation rates from the 2⁰ and 2¹ levels could only proceed by tunneling through this barrier while dissociation from the higher lying levels was described by a 2:1 Fermi resonance of ν_2 directly to the manifold of N-H(D) continuum states lying above the barrier. This model also predicts that photodissociation of NHD₂ should proceed primarily through the NHD+D pathway.

Dissociation of the two lowest vibronic bands was found to have a weak dependence upon rotation level. Rotationally enhanced dissociation from the zero-point level in both NH₃ and ND₃ is caused by the lowering of the effective barrier height by centrifugal forces. The rotational enhancement of the dissociation rate from the NH₃ 2¹ level, which is predicted to lie above the potential barrier along the N-H stretch, was dominated by perpendicular Coriolis coupling to the manifold of continuum states lying above the barrier. The same level in ND₃ lies below the barrier to dissociation and the rotational dependence of the dissociation rates still fits the centrifugal model.¹²

ACKNOWLEDGMENTS

This work is taken in part from the Ph. D. thesis of Steven A. Henck (Ref. 1). This work was supported by a grant from the National Science Foundation.

- ¹S. A. Henck, Ph.D. thesis, Princeton University, 1990.
- ²G. Herzberg, *Molecular Spectra and Molecular Structure: Electronic Spectra and Electronic Structure of Polyatomic Molecules* (Van Nostrand, New York, 1966), Vol. III.
- ³R. Runau, S. D. Peyerimhoff, and R. J. Buenker, *J. Mol. Spectrosc.* **68**, 253 (1977).
- ⁴M. I. McCarthy, P. Rosmus, H. J. Werner, P. Botschwina, and V. Vaida, *J. Chem. Phys.* **86**, 6693 (1987).
- ⁵M. N. R. Ashfold, C. L. Bennett, and R. N. Dixon, *Faraday Discuss. Chem. Soc.* **82**, 163 (1986).
- ⁶R. N. Dixon, *Chem. Phys. Lett.* **147**, 377 (1988).
- ⁷P. Rosmus, P. Botschwina, H. J. Werner, V. Vaida, P. C. Engelking, and M. I. McCarthy, *J. Chem. Phys.* **86**, 6677 (1987).
- ⁸S. L. Tang and D. G. Imre, *Chem. Phys. Lett.* **144**, 6 (1988).
- ⁹S. L. Tang, D. G. Imre, and D. Tannor, *J. Chem. Phys.* **92**, 5919 (1990).
- ¹⁰S. L. Tang, E. V. Abramson, and D. G. Imre, *J. Phys. Chem.* **95**, 4969 (1991).
- ¹¹M. N. R. Ashfold, R. N. Dixon, and R. J. Stickland, *Chem. Phys.* **88**, 463 (1984).
- ¹²M. N. R. Ashfold, C. L. Bennett, and R. N. Dixon, *Chem. Phys.* **93**, 293 (1985).
- ¹³M. N. R. Ashfold, R. N. Dixon, S. J. Irving, H. M. Koeppel, W. Meier, J. R. Nightingale, L. Schnieder, and K. H. Welge, *Philos. Trans. R. Soc. London* **332**, 375 (1990).
- ¹⁴J. Biesner, L. Schnieder, J. Schmeer, G. Ahlers, X. Xie, K. H. Welge, M. N. R. Ashfold, and R. N. Dixon, *J. Chem. Phys.* **88**, 3607 (1988).
- ¹⁵J. Biesner, L. Schnieder, X. Xie, G. Ahlers, K. H. Welge, M. N. R. Ashfold, and R. N. Dixon, *J. Chem. Phys.* **91**, 2901 (1989).
- ¹⁶A. E. Douglas, *Discuss. Faraday Soc.* **35**, 158 (1963).
- ¹⁷Y. Endo, M. Iida, and Y. Ohshima, *Chem. Phys. Lett.* **174**, 401 (1990).
- ¹⁸K. Fuke, H. Yamada, Y. Yoshida, and K. Kaya, *J. Chem. Phys.* **88**, 5238 (1988).
- ¹⁹S. W. Leifson, *Astrophys. J.* **63**, 73 (1933).
- ²⁰V. Vaida, M. I. McCarthy, P. C. Engelking, P. Rosmus, H. J. Werner, and P. Botschwina, *J. Chem. Phys.* **86**, 6669 (1987).
- ²¹A. D. Walsh and P. A. Warshop, *Trans. Faraday Soc.* **57**, 345 (1961).
- ²²J. Xie, G. Sh, X. Zhang, and C. Zhang, *Chem. Phys. Lett.* **124**, 99 (1986).

- ²³L. D. Ziegler and B. Hudson, *J. Phys. Chem.* **88**, 1110 (1984).
- ²⁴A. Nakajima, K. Fuke, K. Tsukamoto, Y. Yoshida, and K. Kaya, *J. Phys. Chem.* **95**, 571 (1991).
- ²⁵L. D. Ziegler, *J. Chem. Phys.* **86**, 1703 (1987).
- ²⁶M. N. R. Ashfold and R. N. Dixon, *Chem. Phys. Lett.* **177**, 597 (1991).
- ²⁷S. A. Henck, M. A. Mason, W.-B. Yan, and K. K. Lehmann, *J. Chem. Phys.* **102**, 4772 (1995).
- ²⁸R. N. Dixon, *Mol. Phys.* **68**, 263 (1991).
- ²⁹C. J. Williams, J. Qiean, and D. J. Tannor, *J. Chem. Phys.* **95**, 1721 (1991).
- ³⁰L. D. Ziegler, *J. Chem. Phys.* **84**, 6013 (1986).